Mathematical Modeling and Algorithm Application
ISSN: 3006-0842 | Vol. 8, No. 3, 2026

Research on Power Generation Forecasting for Photovoltaic Power Plants Based on Spatio-Temporal Multidimensional Feature Decomposition and Deep Learning Architecture

Yan Pan*, Gang Qin

College of Electrical Engineering and New Energy, China Three Gorges University, Yichang 443000, China
* **Corresponding author**: Yan Pan (Email: 13597581295@163.com)

Abstract: Against the backdrop of energy transition driven by the "dual carbon" goals, this study addresses the challenges posed by the fluctuating power output of photovoltaic (PV) generation to grid stability by establishing an integrated forecasting framework combining physical modeling and deep learning. First, a theoretical irradiation and power generation model based on geographic location information was established as an ideal benchmark for deviation analysis. The STL decomposition method was applied to decompose the power sequence into seasonal, trend, and random components, while the K-means clustering algorithm quantified intraday power fluctuation characteristics. Analysis reveals a 55.30% deviation rate between actual and theoretical summer power, highlighting environmental uncertainty impacts. Subsequently, a "month-day-hour" three-dimensional tensor-based data reconstruction technique was introduced. By characterizing multi-scale features through seasonal indices and intraday distribution factors, the performance of LSTM and Transformer models in day-ahead power forecasting was comparatively validated. Experimental results demonstrate that the LSTM model exhibits significant advantages in capturing power variation trends, achieving a low root mean square error of 3.7229%. This effectively addresses the technical challenge of low prediction accuracy under complex meteorological conditions, providing reliable data support for grid dispatch.

Keywords: STL time series decomposition, LSTM forecasting model, Multiscale feature modeling.

1. Introduction

Amidst the global trend toward low-carbon development, photovoltaic power generation has become a core force in China's energy structure transformation[1]. However, its output exhibits strong randomness and volatility due to meteorological factors such as cloud cover, overcast conditions, and seasonal changes, posing severe challenges to grid safety and efficient integration. This study focuses on quantifying PV power characteristics across multiple spatiotemporal scales and developing intraday power forecasting based on temporal feature decomposition and deep neural networks. Previous research has predominantly emphasized unidimensional statistical forecasting, often overlooking the coupling relationship between long-term seasonal patterns and short-term intraday fluctuations in PV output. The innovations of this section are twofold: First, a theoretical power benchmark integrating geographic information and physical constraints was established, achieving refined quantification of output characteristics through STL decomposition and K-means clustering. Second, a multi-factor forecasting architecture based on three-dimensional tensor reconstruction was proposed. By decoupling seasonal indices from intraday distribution factors, this approach enhances the deep learning model's ability to perceive nonlinear fluctuations. The overall research approach follows a progressive logic from physical mechanism modeling to historical data feature extraction, then to deep learning model training and evaluation, aiming to construct a complete technical pathway covering characteristic analysis to precise inversion[2-3].

2. Analytical Model for Seasonal and Intraday Characteristics of Theoretical-Actual Power Coupling

2.1. Model Establishment

2.1.1. Construction of Theoretical Power Model

Based on geographical location (such as longitude, latitude r, plane and panel tilt angle β) and the Earth-Sun relationship, a theoretical irradiation and power model is established as the "ideal benchmark" for deviation analysis[4].

First, the calculation formulas for the declination angle δ and hour angle ω during the Earth's motion around the Sun are established:

$$\delta(n) = 23.45 \cdot \sin\left[\frac{2\pi}{365} \cdot (284 + n)\right] \quad (1)$$

$$\omega(t_{sun}) = 15 \cdot (t_{solar} - 12) \quad (2)$$

Where, $n \in [1,365]$ represents the nth day of the year, reflecting the impact of seasonal changes on the irradiation angle; t_{sun} is the solar time (unit: hours), depicting the diurnal change of the irradiation direction.

Second, the calculation formulas for the solar altitude angle h and solar azimuth angle α are established:

$$h(t) = \arcsin(\sin\phi \cdot \sin\delta + \cos\phi \cdot \cos\delta \cdot \cos\omega) \quad (3)$$

$$\alpha(t) = \arccos\left(\frac{\sin\delta \cdot \cos\phi - \cos\delta \cdot \sin\phi \cdot \cos\omega}{\cosh}\right) \quad (4)$$

Where, δ is the declination angle, ω is the hour angle, and ϕ is the longitude.

Ignoring atmospheric scattering, the direct solar radiation intensity $G(t)$ received per unit area is estimated based on the solar altitude angle:

$$G(t) = G_{sc} \cdot [\sin(h(t)) \cdot \cos\beta + \cos(h(t)) \cdot \sin\beta \cdot \cos(\alpha(t) - \gamma)] \quad (5)$$

Where, G_{sc} is the solar constant, $\alpha(t)$ is the solar azimuth angle, and γ is the panel azimuth angle.

Establishment of the theoretical power function:

$$P_{th}(t) = \eta \cdot A \cdot G(t) \quad (6)$$

Where, η is the efficiency of the photovoltaic module ($0 < \eta < 1$), and A is the total area of the module (unit: m^2).

2.1.2. STL Decomposition to Reveal Seasonal Patterns

Aiming at the multi-scale fluctuation characteristics of the photovoltaic power sequence, the STL method is adopted to decompose it into seasonal components, trend components, and random components. By calculating the variance ratio of the seasonal components, the characteristics of long-term seasonal fluctuations on power changes are analyzed[5].

Step 1: Preprocessing Steps.

Remove samples where the power value exceeds 120% of the installed capacity or is lower than -5%.

Use cubic spline interpolation to repair short-term missing data to ensure sequence continuity.

Step 2: STL Decomposition Process.

Establishment of the STL model:

$$P(t) = S(t) + T(t) + R(t) \quad (7)$$

Where, $P = \{p_1, p_2, \ldots, p_t\}$ is the annual power sequence, and $T = 365 \times 96 = 35040$ (sampling every 15 minutes, 96 points per day during the daytime).

Seasonal component $S(t)$: Extracted through a 365-day sliding window, reflecting the average power at the same season and time, such as the power at noon in summer is significantly higher than that in winter.

Trend component $T(t)$: Extract long-term changes through LOESS smoothing.

Random component $R(t)$: Including short-term meteorological disturbances, measurement errors, etc.

Step 3: Quantitative Analysis.

Perform seasonal extraction, calculate the moving average using a sliding window of 365 days, and extract $S(t)$. The expression is:

$$S(t) = \frac{1}{2M+1} \sum_{k=-M}^{M} P(t+k), M = 182 \text{ (symmetric window)} \quad (8)$$

Apply LOESS smoothing to the deseasonalized sequence $P(t) - S(t)$ with a window width of 30 days, iteratively fit the trend $T(t)$, and calculate the random component:

$$R(t) = P(t) - S(t) - T(t) \quad (9)$$

Step 4: Quantitative Analysis of Seasonal Contribution.

Calculate the variance ratio of the seasonal components:

$$\text{Contribution Rate} = \frac{\text{Var}(S)}{\text{Var}(P)} \times 100\% \quad (10)$$

If the contribution rate exceeds 60%, it indicates that seasonality is the main source of fluctuation.

Calculate the Pearson correlation coefficient between the seasonal component $S(t)$ and the theoretical irradiation I_{th}:

$$\rho = \frac{\sum_{t=1}^{T} [S(t) - \bar{S}](I_{th} - \bar{I})}{\sqrt{\sum_{t=1}^{T} [S(t) - \bar{S}]^2 \sum_{t=1}^{T} (I_{th} - \bar{I})^2}} \quad (11)$$

Where, $I_{th} = \{i_1, i_2, \ldots, i_T\}$ is the corresponding theoretical irradiation intensity sequence.

Calculate the Pearson correlation coefficient ρ between $S(t)$ and the theoretical irradiation $I_{th}(t)$. If $|\rho| > 0.8$, the hypothesis that irradiation dominates seasonal fluctuations is verified.

2.1.3. Cluster Analysis of Short-Term Characteristic Laws

Step 1: Multi-Dimensional Features of Diurnal Power Curves

For each diurnal sample, extract the following $D = 7$-dimensional features:

$$\mu = \frac{1}{96} \sum_{i=1}^{96} p_i \quad (12)$$

$$CZ = \max(p_i) - \min(p_i) \quad (13)$$

$$\sigma = \sqrt{\frac{1}{96} \sum_{i=1}^{96} (p_i - \mu)^2} \quad (14)$$

Where, μ is the mean value, σ is the standard deviation, and CZ is the peak-valley difference.

$$t_{peak} = \arg\max(p_i) \quad (15)$$

$$PD = \frac{1}{96} \sum_{i=1}^{96} \left(\frac{p_i - \mu}{\sigma}\right)^3 \quad (16)$$

$$BDS = -\sum_{i=1}^{96} \left(\frac{p_i}{\sum p_i}\right) \ln\left(\frac{p_i}{\sum p_i}\right) \quad (17)$$

Where, t_{peak} is the peak time, PD is the skewness, and BDS is the fluctuation entropy.

Step 2: Construction of K-means Clustering Model

Construct an objective function to minimize the sum of squared intra-class distances:

$$\min_{c_1,\ldots,c_k} \sum_{K=1}^{K} \sum_{x \in C_k} \|x - \mu_k\|_2^2 \quad (18)$$

Where, μ_k is the centroid of the k-th cluster, and C_k is the sample set of the k-th cluster.

Randomly initialize k centroids μ_k^{t+1}. For each sample x_i, assign it to the class C_k of the nearest centroid. Recalculate the class centroid $\mu_k^{(t+1)} = \frac{1}{|C_k|} \sum_{x_i \in C_k} x_i$. Repeat steps 2-3 until the centroids no longer change significantly or the maximum number of iterations is reached.

Calculate the average deviation rate between the actual power and the theoretical power for each cluster:

$$\text{Bias}_k = \frac{1}{n_k} \sum_{x \in C_k} \frac{P_{ac} - P_{th}}{P_{th}} \times 100\% \quad (19)$$

Evaluate the clustering quality by calculating the average silhouette coefficient $\bar{s}$. The formula is:

$$\bar{S} = \frac{1}{N} \sum_{i=1}^{N} \frac{b_i - a_i}{\max(a_i, b_i)} \quad (20)$$

Where, a_i is the average intra-class distance of sample i, and b_i is the average distance from sample i to the nearest class. The closer $\bar{s}$ is to 1, the better the clustering effect.

Through the above modeling process, the long-term seasonal laws and short-term weather-driven patterns of photovoltaic power can be systematically analyzed, providing feature inputs and error correction basis for the prediction

models of Problems 2 to 4.

2.2. Model Solution

2.2.1. Solution of Long-Term Seasonal Power Generation

Based on parameters such as longitude, latitude, and panel tilt angle, the theoretical irradiation intensity of each season is calculated through formulas for declination angle, hour angle, solar altitude angle, and azimuth angle. Then, the theoretical power generation model is solved by combining the module efficiency and area to obtain the theoretical power generation of the photovoltaic power station. Thus, the average deviation rate between the actual power and the theoretical power of each season is calculated. The solution results are visualized to obtain Table 1, and the seasonal variation characteristics of the photovoltaic power station's power generation are analyzed by combining the STL decomposition method.

Table 1 Power Generation Characteristics of Each Season

Season	Average Theoretical Power (MW)	Average Actual Power (MW)	Average Irradiation Intensity (W/m²)	Deviation Rate (%)
Spring	6.36	3.40	153.20	-46.55%
Summer	2.98	4.56	246.13	52.96%
Autumn	2.41	3.74	228.26	55.29%
Winter	4.27	3.00	112.13	-29.77%

2.2.2. Solution of Short-Term Diurnal Fluctuation Power Generation

According to the irradiation intensity standards under different weather conditions, the solution results of the theoretical power generation model are screened to obtain the theoretical power generation at each time under different weather conditions.

2.3. Result Analysis

2.3.1. Analysis of Long-Term (Seasonal Change) Power Generation Characteristics

By comparing the theoretical power generation obtained from the solution of the theoretical power model in each season with the actual power generation, and graphically processing the calculated average deviation between the actual power and the theoretical power in each season, the following Figure 1 is obtained.

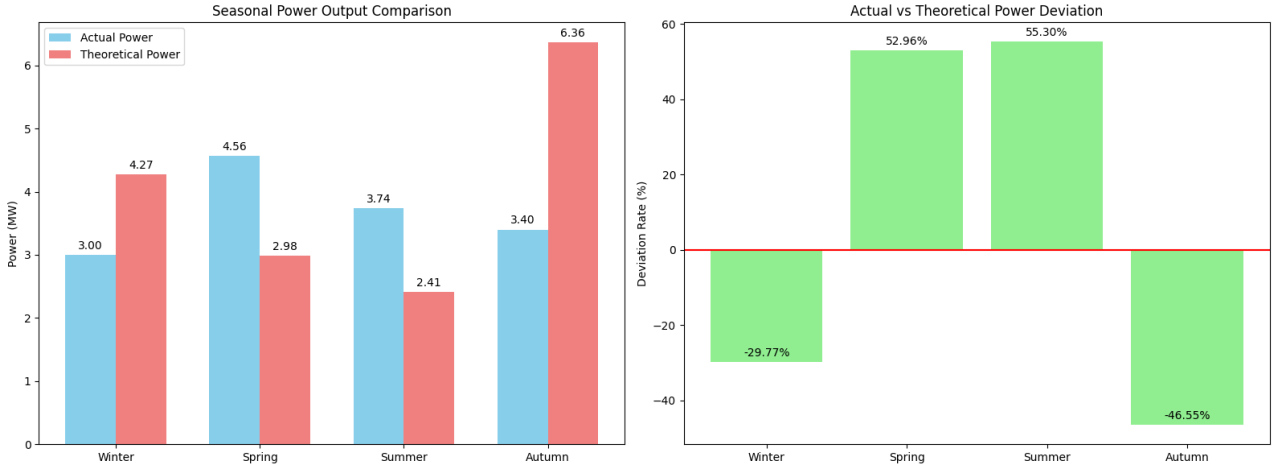

Figure 1 Power Generation Characteristics of Each Season

It can be seen from the above figure that in terms of the comparison of seasonal power generation, the power generation of the photovoltaic power station shows significant seasonal differences, which are specifically manifested as follows:

Summer: Both the actual power and the theoretical power are the highest among the four seasons, reaching 6.36MW and 60MW respectively. In summer, the solar altitude angle is large, the daytime is long, the solar irradiation intensity is high and lasts for a long time, so that the total solar radiation received by the photovoltaic panels is the largest, driving the power generation to reach the peak.

Spring: The actual power is 4.27MW, and the theoretical power is 45MW, second only to summer. In this season, the solar irradiation intensity gradually increases, and the daytime is longer than that in winter, providing good lighting conditions for power generation.

Autumn: The actual power drops to 3.74MW and 3.40MW, and the theoretical power is 29.8MW and 24.1MW respectively. With the progress of the season, the solar altitude angle decreases, the daytime becomes shorter, and both the solar irradiation intensity and the lighting time decrease, leading to a significant reduction in power generation. Moreover, the autumn data of different years fluctuates greatly, which may be related to the uncertainty of meteorological factors such as cloudy and rainy weather and haze in autumn.

Winter: The actual power and the theoretical power are the lowest (winter data is not clearly marked in the figure, but it can be inferred from the seasonal laws). The solar irradiation

intensity is the weakest, and the daytime is the shortest, which are the main factors restricting the power generation of the photovoltaic power station.

In terms of the deviation between the actual power and the theoretical power, the deviation rate in summer is 55.30%, 52.96% in spring, and -29.77% and -46.55% in autumn respectively (a negative deviation indicates that the actual power is more lower than the theoretical value).

2.3.2. Analysis of Short-Term (Diurnal Fluctuation) Power Generation Characteristics

Combined with the power generation principle of the photovoltaic power station and meteorological laws, the diurnal power fluctuation shows the following characteristics:

From sunrise to noon: As the solar altitude angle increases, the irradiation intensity gradually enhances, and the power generation shows an upward trend, reaching the peak around noon.

From noon to sunset: The solar altitude angle decreases, the irradiation intensity weakens, and the power generation gradually decreases.

Fluctuation interference factors: Diurnal changes in cloud cover, sudden rainy weather, etc., will cause short-term sharp fluctuations in power. For example, when the sun is blocked by clouds, the actual power may deviate from the theoretical power curve rapidly.

2.3.3. Summary of Power Station Generation Characteristics

The power generation of the photovoltaic power station is dominated by the long-term (seasonal) and short-term (diurnal) changes of solar irradiation. At the same time, it is affected by factors such as meteorological conditions and equipment performance, and there is a significant deviation between the actual power and the theoretical power. In the subsequent modeling, the following points need to be focused on:

Seasonal characteristics: Introduce seasonal time features (such as months and solar terms) as model inputs to improve the prediction accuracy of long-term trends.

Meteorological sensitivity: Combine real-time forecast information such as irradiation and cloud cover in NWP data to dynamically correct the prediction of short-term power fluctuations.

3. LSTM-Transformer Contrastive Forecasting Model with Multi-Scale Time Feature Fusion

3.1. Establishment of Power Generation Prediction Model

3.1.1. Data Preprocessing

First, perform structured processing on the data, divide it by "month-date-time", eliminate outliers, and repair short-term missing values. The training set and test set are divided according to the document rules: the last week of the 2nd, 5th, 8th, and 11th months are the test set, and the rest are the training set.

According to the requirements of Table 1 in the document, the historical power data should have a time resolution of 15 minutes and cover the whole year. It can be known from the modeling of Problem 1 that the obtained data set is:

$$\mathrm{P} = \{\mathrm{p}_1, \mathrm{p}_2, \ldots, \mathrm{p}_\mathrm{T}\}, \mathrm{T} = 35040 \tag{21}$$

Reorganize into a three-dimensional structure by "month-day-time":

$$\mathrm{P}(\mathrm{m}, \mathrm{d}, \mathrm{t}) \tag{22}$$

Where, m represents the month, d represents a certain day of the m-th month, and t represents the time within the day.

According to the operating characteristics of photovoltaic equipment, the power value of photovoltaic equipment should satisfy $0 \le \mathrm{P} \le 1.1\mathrm{C}$. For data points beyond this range, the mean value interpolation of adjacent times is used for repair:

$$\mathrm{p}_{\mathrm{fix}}(\mathrm{t}) = \frac{\mathrm{p}(\mathrm{t}-1) + \mathrm{p}(\mathrm{t}+1)}{2} \tag{23}$$

Where, C is the installed capacity of the photovoltaic equipment.

3.1.2. Long-Term Modeling

Calculate the seasonal index S_m, which is the ratio of the average daily power of each month to the annual average, through the training set to quantify the deviation degree of the power of each month relative to the annual average, reflecting the long-term seasonal changes of solar irradiation. For example, S_m in summer is usually greater than 1, and vice versa in winter. The formula for S_m is:

$$\mathrm{S}_\mathrm{m} = \frac{\overline{\mathrm{p}}_{\mathrm{month}}(\mathrm{m})}{\overline{\mathrm{p}}_{\mathrm{annual}}(\mathrm{m})} \tag{24}$$

$\overline{\mathrm{p}}_{\mathrm{month}}(\mathrm{m})$ is the average daily power of the training set in the m-th month. The formula is:

$$\overline{\mathrm{p}}_{\mathrm{month}}(\mathrm{m}) = \frac{1}{\mathrm{N}_\mathrm{m} \times 96} \sum_{\mathrm{d}=1}^{\mathrm{N}_\mathrm{m}} \sum_{\mathrm{t}=1}^{96} \mathrm{P}(\mathrm{m}, \mathrm{d}, \mathrm{t}) \tag{25}$$

Where, N_m is the number of days in the training set of the m-th month. $\overline{\mathrm{p}}_{\mathrm{annual}}(\mathrm{m})$ is the average daily power of the annual training set. The formula is:

$$\overline{\mathrm{p}}_{\mathrm{annual}} = \frac{1}{337 \times 96} \sum_{\mathrm{m}=1}^{12} \sum_{\mathrm{d}=1}^{\mathrm{N}_\mathrm{m}} \sum_{\mathrm{t}=1}^{96} \mathrm{P}(\mathrm{m}, \mathrm{d}, \mathrm{t}) \tag{26}$$

3.1.3. Short-Term Modeling

The diurnal distribution factor $\mathrm{D}(\mathrm{m})$ is used to describe the proportion of power at each time within the m-th month to the average daily power, reflecting the power change law of "sunrise-noon-sunset". For example, $\mathrm{D}(\mathrm{m})$ on sunny days is unimodal with the peak at noon, while on cloudy days, there may be multi-peak fluctuations. The formula for $\mathrm{D}(\mathrm{m})$ is:

$$\mathrm{D}_\mathrm{m}(\mathrm{t}) = \frac{\overline{\mathrm{P}}_{\mathrm{day}}(\mathrm{m}, \mathrm{t})}{\overline{\mathrm{P}}_{\mathrm{month}}(\mathrm{m})} \tag{27}$$

$$\sum_{\mathrm{t}=1}^{96} \mathrm{D}_\mathrm{m}(\mathrm{t}) = 96 \tag{28}$$

$\overline{\mathrm{P}}_{\mathrm{day}}(\mathrm{m}, \mathrm{t})$ is the average power at the t-th time in the training set of the m-th month. The formula is:

$$\overline{\mathrm{P}}_{\mathrm{day}}(\mathrm{m}, \mathrm{t}) = \frac{1}{\mathrm{N}_\mathrm{m}} \sum_{\mathrm{d}=1}^{\mathrm{N}_\mathrm{m}} \mathrm{P}(\mathrm{m}, \mathrm{d}, \mathrm{t}) \tag{29}$$

To suppress noise and retain physical rationality, a 3-time moving average is performed on $\mathrm{D}_\mathrm{m}(\mathrm{t})$:

$$\mathrm{D}'_\mathrm{m}(\mathrm{t}) = \begin{cases} \dfrac{\mathrm{D}_\mathrm{m}(\mathrm{t}-1) + \mathrm{D}_\mathrm{m}(\mathrm{t}) + \mathrm{D}_\mathrm{m}(\mathrm{t}+1)}{3}, & \mathrm{t} = 2 \sim 95, \\ \mathrm{D}_\mathrm{m}(\mathrm{t}), & \mathrm{t} = 1 \text{ or } 96 \end{cases}, \mathrm{D}'_\mathrm{m} \in [0, 1.1] \tag{30}$$

3.1.4. Construction of LSTM Prediction Model

Take the historical window length L and construct the input vector:

$$\tilde{P}_t = \left[P_{t-L+1}, P_{t-L+2}, \ldots, P_t, S_{m(t)}\right]^T \in R^{(L+1)\times 1} \quad (31)$$

Where, $m_{(t)}$ is the month corresponding to time t, and $S_{m(t)}$ is the real-time seasonal index.

Let the dimension of the LSTM hidden layer be n_k. The update formulas of the forget gate f_t, input gate i_t, output gate o_t, and cell state c_t are:

$$\begin{cases} f_t = \sigma(W_f X_t + U_f h_{t-1} + b_f) \\ i_t = \sigma(W_i X_t + U_i h_{t-1} + b_i) \\ \tilde{c}_t = \tanh(W_c X_t + U_c h_{t-1} + b_c) \\ c_t = f_t \odot c_{t-1} + i_t \odot \tilde{c}_t \\ h_t = o_t \odot \tanh(c_t) \\ o_t = \sigma(W_o X_t + U_o h_{t-1} + b_o) \end{cases} \quad (32)$$

Where, σ is the Sigmoid function, $\odot$ is the element-wise product, and $h_t \in R^{n_k}$.

Map the hidden state to the prediction space through the fully connected layer:

$$\hat{p}_f(m,d,t) = W_{out} \cdot h_t + b_{out}, \hat{p}_f(m,d,t) \in R^N \quad (33)$$

Where, $\hat{p}_f(m,d,t)$ is the future prediction sequence, satisfying $\hat{p}_f(m,d,t+i) = \hat{T}_{t+i} \cdot S_{m(t+i)}$.

3.1.5. Construction of Transformer Prediction Model

Encode the historical power sequence and seasonal index into a multi-dimensional vector:

$E_t = \text{Embedding}(P_{t-L+1:t}) + \text{PosEncoding}(t) + \text{Embedding}(t) + \text{Embe}$

Let d_{model} be the model dimension, and determine the position encoding:

$$\text{PosEncoding}(t, 2j+1) = \cos\left(\frac{t}{10000^{2j/d_{model}}}\right), j \in \{1,2,\ldots,d_{model}/2\} \quad (35)$$

$$\text{PosEncoding}(t, 2j) = \sin\left(\frac{t}{10000^{2j/d_{model}}}\right) \quad (36)$$

Establish the multi-head self-attention mechanism:

$$\text{MultiHead}(Q,K,V) = \text{Concat}(\text{head}_1, \ldots, \text{head}_h)W_O \quad (37)$$

$$\text{head}_i = \text{Softmax}\left(\frac{QK_i^T}{\sqrt{d_k}}\right)V_i \quad (38)$$

Where, $Q = K = V = E_t$, $h = 8$, and the dimension of a single head $d_k = d_{model}/h$.

Feed-forward network and output:

$$\text{FFN}(X) = \sigma(XW_1 + b_1)W_2 + b_2 \quad (39)$$

After extracting features through multiple Encoder layers, generate the prediction sequence through the Decoder:

$$\hat{P}_{Tra} = \text{Linear}(\text{DecoderOut}) \quad (40)$$

The Decoder adopts a masked self-attention mechanism to avoid future information leakage.

3.2. Evaluation of Prediction Models

Calculate the root mean square error E_{rmse} to reflect the overall deviation degree between the predicted value and the actual value. The formula is:

$$E_{rmse} = \sqrt{\frac{1}{2688}\sum_{(m,d,t)\in T_{test}}\left(\frac{P(m,d,t) - \hat{P}_f(m,d,t)}{C_t}\right)^2} \quad (41)$$

Where, C_t is the installed capacity of the photovoltaic equipment at time t, and T_{test} is the test set. $\hat{P}_f(m,d,t) \in [0,1.1C]$.

Calculate the mean absolute error E_{mae} to measure the average of the absolute values of the prediction errors. The formula is:

$$E_{mae} = \frac{1}{2688}\sum_{(m,d,t)\in T_{test}}\left|\frac{P(m,d,t) - \hat{P}_f(m,d,t)}{C_t}\right| \quad (42)$$

Where, $\overline{P}(m,d,t)$ is the actual average value, and $\hat{P}_f(m,d,t)$ is the predicted average value.

3.3. Model Solution

Use the training set data to train the LSTM prediction model and the Transformer prediction model. Take the data of the last week of the 2nd, 5th, 8th, and 11th months as the test set to solve the LSTM prediction model and the Transformer prediction model, and obtain the power generation prediction data of the last week under the two prediction models. Organize the data and perform visualization processing to obtain the power prediction result table of the last 7 days of the 2nd, 5th, 8th, and 11th months. Taking the second month (July 2018) as an example, the power prediction results of the last 7 days are shown in Table 2 below. The complete prediction data is detailed in the appendix.

Table 2 Power Prediction Results of the Last 7 Days of the 2nd Month

Start Time	Forecast Time	Actual Power (MW)	Predicted Power by LSTM Model (MW)	Predicted Power by Transformer Model (MW)
2018/7/25/12:45	2018/7/25/13:00	0	-0.071179	0.640763
2018/7/25/12:45	2018/7/25/13:15	0	-0.364087	0.424937
2018/7/25/12:45	2018/7/25/13:30	0	-0.417525	0.695646
2018/7/25/12:45	2018/7/25/13:45	0	-0.260975	0.367016
2018/7/25/12:45	2018/7/25/14:00	0	-0.003434	0.415260
...	...	...	...	...
2018/7/30/10:15	2018/7/31/13:30	0	1.085285	4.017019
2018/7/30/10:15	2018/7/31/13:45	0	0.591773	3.801084
2018/7/30/10:15	2018/7/31/14:00	0	0.287412	3.098429

Test the prediction models and evaluate their accuracy. Calculate the root mean square error E_{rmse}, mean absolute percentage error E_{mape}, and error coefficients. The error coefficient values of the two prediction models obtained by solving are as table 3.

Table 3 Error Coefficient Values of Prediction Models

Prediction Model	Error Coefficient Values (%)		
	E_{rmse}	E_{mae}	E_{mape}
LSTM Prediction Model	3.7229	2.9353	89.3472
Transformer Prediction Model	6.0830	5.2726	194.1290

3.4. Result Analysis

Graphically process the power generation prediction data of the last week under the two prediction models to obtain Figure 2.

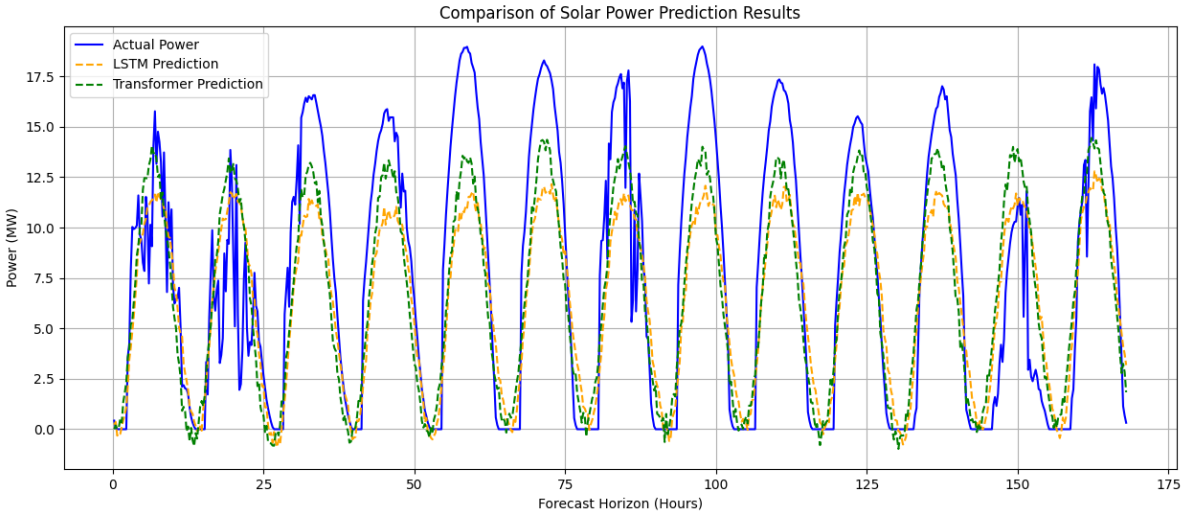

Figure 2 Power Prediction Results of the Two Models Based on Historical Data

Overall Trend Fitting Degree:

The prediction curve of the Transformer model fits well with the actual power curve in most periods and can better follow the fluctuation trend of the actual power, indicating that it has a strong ability to grasp the change trend of photovoltaic power generation. Although the prediction curve of the LSTM model can also reflect the power change trend, the deviation from the actual curve is relatively obvious. Especially in the stage of rapid power rise and fall, the LSTM model has a response lag and poor fitting degree.

Accuracy of Peak and Valley Prediction:

At the peak and valley of power, the predicted value of the Transformer model is closer to the actual value, which can relatively accurately capture the time and value of the power extreme value, and the prediction accuracy is higher. The predicted value of the LSTM model has a large deviation from the actual value at the peak and valley of power, and there is an underestimation or overestimation phenomenon, so the accuracy of predicting extreme values is poor.

Ability to Capture Fluctuation Details:

The Transformer model has a strong ability to capture the details of power fluctuations and can timely reflect the rapid changes in power. The fluctuation of the prediction curve is basically consistent with that of the actual curve, indicating

that it performs well in dealing with complex power change situations. However, the LSTM model is insufficient in capturing the details of power fluctuations, and the prediction curve is relatively smooth, which cannot well reflect the rapid changes in power. In the periods of frequent fluctuations, the prediction accuracy is affected.

In summary, the Transformer model is superior to the LSTM model in the accuracy of predicting photovoltaic power generation, but both have room for improvement. In the future, the prediction accuracy can be improved by optimizing model parameters or improving the structure.

4. Conclusions

This study systematically analyzes the output characteristics of photovoltaic power plants and establishes a day-ahead prediction model. By constructing a theoretical irradiance model, we identified and quantified deviation characteristics of PV power output across seasons and weather conditions, revealing the physical mechanisms behind high summer output and high autumn variability. Comparative analysis of LSTM and Transformer models confirmed that incorporating seasonal indices and intraday distribution factors significantly improves prediction stability, with LSTM demonstrating superior engineering applicability through lower error metrics.

Limitations and Future Research Prospects

Although this model achieves good results in trend capture and accuracy control, certain limitations remain. The current theoretical model neglects practical external factors such as the temperature effect of photovoltaic modules, surface dust loss, and terrain shading, resulting in an incomplete analysis of deviations between theory and actual measurements. Additionally, the computational complexity of deep learning models and algorithms like Kriging interpolation creates bottlenecks when processing large-scale real-time data. Future research will focus on incorporating temperature correction models and dust accumulation loss factors to refine theoretical benchmarks. We will also explore frequency domain optimization techniques, such as those based on the Fast Fourier Transform (FFT), to enhance algorithmic efficiency. Furthermore, we aim to extend the multimodal fusion model to broader renewable energy applications, including agricultural weather forecasting and wind power generation.

References

[1] Ijačić A, Špago D, Spaić O, et al. Forecasting Electicity in Photovoltaic Power Plants[J]. B& H Electrical Engineering, 2025, 19(2):1-7.

[2] Pan J, Qian J, Cao M. DAY-AHEAD PREDICTIONS OF THE POWER GENERATED BY A PHOTOVOLTAIC POWER PLANT[J]. World Journal of Engineering Research, 2025,3(4).

[3] Miao Z, Shao J, Lin B, et al. Prediction of stable power generation period of photovoltaic power station based on time series ARIMA model[J]. Journal of Physics: Conference Series, 2025, 2993(1): 012003-012003.

[4] Liao R, Liu Y, Xu X, et al. Enhanced photovoltaic power generation forecasting for newly-built plants via Physics-Infused transfer learning with domain adversarial neural networks[J]. Energy Conversion and Management, 2024, 322119114-119114.

[5] Haljasmaa I K, Bramm M A, Matrenin V P, et al. Weather Condition Clustering for Improvement of Photovoltaic Power Plant Generation Forecasting Accuracy[J]. Algorithms, 2024, 17(9): 419-419.